https://doi.org/10.5194/egusphere-2026-3940
Preprint. Discussion started: 28 July 2026

Mongolian Cyclone Intensification Reshapes Dust Activity in Northwest China

Wenhui Zhang[1], Zhengcai Zhang[1,2,3*], Lingguang Zhang[1], Zhenyu Zhang[1], Yunzhu Lei[1], Siqi Wang[1], Pan Fang[1], Zhibao Dong[1,2,3], Lanying Han[1,2,3], Wenshu Wang[4], Limin Yuan[5]

[1]School of Geography and Tourism, Shaanxi Normal University, Xi'an, 710119, China
[2]Key Laboratory of Qian Xuesen Deserticulture of Shaanxi Higher Education Institute, Xi'an, 710119, China
[3]Yulin Desert-Loess Transition Zone Ecology and Environment Shaanxi Provincial Field Scientific Observation Station, Xi'an, 710119, China
[4]Alxa Forestry and Grassland Research Institute, Alxa 750306, China
[5]Inner Mongolia Forestry Science Research Institute, Hohhot 010000, China

Correspondence to: Zhang Zhengcai (zhangzhengcai@snnu.edu.cn) and Han Lanying (hanly@snnu.edu.cn)

Abstract. Dust storms are a common hazardous weather phenomenon in arid regions. In recent years, dust storm intensity in northwest China has increased markedly under changing atmospheric circulation conditions, yet the underlying mechanisms remain debated. Previous studies have largely attributed dust variability to land-surface changes and broad-scale circulation anomalies, but the spatially divergent responses of different dust source regions to circulation changes remain poorly understood. Here, we investigate Mongolian cyclone variability during 2001–2025 and its impacts on dust activity in the Taklimakan Desert, Alxa Plateau, and Mu Us Sandy Land using multi-source observational data and a random forest regression model. Results showed that (1) Mongolian cyclone intensity increased from 94.84×10^{-5} s^{-1} to 97.76×10^{-5} s^{-1} and shifted southward by about 2.08° after 2019; (2) Strengthened Mongolian cyclone activity enhanced dust emissions in the Alxa Plateau (from 0.23 to 0.28 $g \cdot m^{-2}$ since 2019), whereas dust activity declined in the Taklimakan Desert, which is less affected by Mongolian cyclone forcing (from 0.63 to 0.57 $g \cdot m^{-2}$ since 2019); (3) Wind was the dominant driver of dust activity (contribution >0.60), while precipitation and the Pressure Gradient Index (PGI) were important secondary contributors in the Alxa and Mu Us regions, and PGI partially modulated wind effects in surrounding cities; and (4) Regional spring mean PM_{10} concentrations are projected to increase substantially during 2026–2100 (229.98–824.31 $\mu g \cdot m^{-3}$) and show weak sensitivity to emission scenarios. These findings highlight the importance of explicitly considering cyclone-wind regime-topography interactions in future dust projections, as circulation-driven variability may play a larger role than previously recognized in regulating East Asian dust activity.

Keywords. Dust storm, Mongolian cyclone, PM_{10} concentration, Spatiotemporal variation, Meteorological factors, Land surface characteristics

https://doi.org/10.5194/egusphere-2026-3940
Preprint. Discussion started: 28 July 2026

1 Introduction

Dust storms are a typical extreme weather in arid areas. Driven by large-scale atmospheric circulation and weather systems, accelerate land desertification, cause severe air pollution, and pose significant risks to human health and urban transportation (Gao et al., 2024; Victor et al., 2024; Wang et al., 2025b; Zhang et al., 2024). Dust particles alter the Earth's radiation balance (Li and Wang, 2022), affect marine biogeochemical cycles (Bishop et al., 2002; Falkowski et al., 1998), and exacerbate respiratory and cardiovascular diseases (Goudie, 2014; Tam et al., 2012; Tong et al., 2023). In April 2025 alone, a major dust storm caused estimated economic losses of 0.08–3.50 billion RMB in China (Zhang et al., 2025).

China accounted for nearly 75% of East Asian dust emissions during spring 2018–2020 (Zhang et al., 2024). However, a recent study based on source apportionment suggested that Mongolia has become an increasingly dominant source, contributing about 43% of East Asian dust in the early 2000s, about 53% in recent years, and as much as 62% in 2022 (Xing et al., 2025). Anomalous warming in the northwest Atlantic combined with eastern Pacific cooling (La Niña) has reduced precipitation and dried soils in Mongolia, enhancing dust emissions (An et al., 2018; Hu et al., 2023). Approximately 88% of severe dust storms in China are driven by Mongolian cyclones (Gao et al., 2024), a proportion much higher than that associated with cold fronts or other systems (Wu et al., 2016; Yu et al., 2023). Poleward cold air intrusion altered sea level pressure patterns, leading to divergent dust variations between the Tarim Basin and the Alxa Plateau (An et al., 2018). Anomalous cyclonic circulation accompanied by upper-level intensified northwesterly wind and intensified surface wind speed (Luo et al., 2026). Since 2021, the intensity and frequency of dust storms in China have risen noticeably (Filonchyk, 2022; Wu et al., 2025). These contrasting findings raise a central question: how the Mongolian cyclone activity governs the spatial variations of dust storm occurrence in dust sources in China.

Although it is well recognized that dust occurrence is controlled by both land surface properties (Pu and Jin, 2021; Wu et al., 2022; Zan et al., 2025) and Mongolian cyclone activity (Yu et al., 2023), few studies have explicitly quantified how cyclone activity modulates surface wind, precipitation, soil moisture, and vegetation, and how these pathways differ across regions. The Tarim Basin (Taklimakan Desert) and the Alxa Plateau (including Mu Us Sandy Land) offer a compelling comparative case study. As the main dust source region in Central Asia, the Tarim Basin is topographically sheltered and minimally affected by Mongolian cyclones, whereas the Alxa Plateau lies directly in the path of northwesterly winds associated with cyclone activity (Han et al., 2025; Yang et al., 2014). Moreover, the post-2021 resurgence of severe dust storms (Wu et al., 2025; Yu et al., 2023) contradicts the persistent greening trend in northern and northwestern China (Fu et al., 2026). This apparent contradiction underscores the need to reanalyze Mongolian cyclone activity on dust occurrence. However, a comprehensive evaluation of the Mongolian cyclone activity effect on spatial variation of dust occurrence remains lacking.

PM_{10} is defined as particulate matter with aerodynamic diameter less than 10 μm, can be transported globally, had greatly effect on climate and environment. Recently, certain progress has been made regarding on the influencing factors and trends of PM_{10} concentrations in China. It is generally accepted that PM_{10} concentrations are primarily driven by factors such as wind speed, precipitation, soil moisture, and land cover (Fu et al., 2026; Pu and Jin, 2021; Wu et al., 2022; Zan et al., 2025).

Wind serves as the key driver of dust transport, and the upper-level westerly jet stream can provide short-term precursor signals for dust storms in northern China (Liu et al., 2004). Vegetation coverage covered land surface and increased land surface roughness length, can reduce about 32.5% dust emission for coverage <15% (Fu et al., 2026). Meanwhile, increased precipitation and soil moisture may promote soil crust formation, thereby limiting dust emissions (Engelstaedter et al., 2003; Liu et al., 2004). Additionally, topography also influences the transport pathways of dust (White et al., 2024; Zhang et al., 2022; Zhang and Dong, 2023). However, current research predominantly focuses on individual dust storm events, with a lack of studies examining trends over the past 45 years.

Building on this foundation, we propose two hypotheses: first, that the influence of the Mongolian cyclone on dust activity differs between the Taklimakan Desert and the Alxa Plateau; and second, that the mechanisms governing dust emissions and transport vary between the interior of desert areas and their surrounding regions (Yu et al., 2023). In summary, significant controversy remains regarding the dominant dust sources and primary driving mechanisms of dust storms in northwest China, highlighting the need for further systematic research. To test these hypotheses, we divide the dust source into two subregions: source 1, the Tarim Basin (Taklimakan Desert), source 2, the Alxa Plateau and Mu Us Sandy Land. These subregions are characterized by distinct near-surface wind regimes, northeasterly winds dominate in the Taklimakan Desert, while the Alxa Plateau and adjacent areas are primarily influenced by northwesterly winds associated with the Mongolian cyclone. In this study, we investigate the characteristics of dust storms day and PM_{10} concentration (grain size smaller than 10 μm) in northwestern and northern China by examining variations in the Mongolian cyclone, supported by an analysis of meteorological factors and land surface conditions. The objective is to provide a scientific basis for developing more targeted strategies for dust prevention and mitigation.

2 Study area and data

2.1 Study area

The study area is located in northwest China. Most areas in northwest China are arid and semi-arid regions, and dust events occur frequently in spring (Liu et al., 2020). There are four dust storm centers and origins in China, Hexi Corridor in Gansu Province and Alxa Plateau in Inner Mongolia, Taklimakan Desert and its surroundings in the south of Xinjiang Autonomous Region, northern slope of Yinshan Mountains in Inner Mongolia and Hunshandake Desert and its surrounding areas, along the Great Wall in Inner Mongolia, Shanxi Province and Ningxia Hui Autonomous Region (Liu et al., 2025, 2020).

2.2 Data

Hourly PM_{10} concentration data were obtained from China National Environment Monitoring Centre (CNEMC: https://www.cnemc.cn/). It currently collects atmospheric pollutants across 367 cities in China. We downloaded the national PM_{10} concentration data for the winter and spring seasons from 2016 to 2025 to analyze temporal trends and spatial

https://doi.org/10.5194/egusphere-2026-3940
Preprint. Discussion started: 28 July 2026

variations in PM_{10} concentrations. We defined the occurrence of dust storms based on a daily PM_{10} concentration exceeding 500 $\mu g \cdot m^{-3}$.

Dust column mass density data was from MERRA-2 dataset (https://disc.gsfc.nasa.gov/datasets/M2TMNXAER_5.12.4/summary) (Global Modeling and Assimilation Office and Pawson, 2015). MERRA, a product of NASA's Global Modeling and Assimilation Office (GMAO), are the results of global atmospheric modeling done with assimilation of observational data. M2T1NXAER (or tavg1_2d_aer_Nx) is an hourly time-averaged 2-dimensional data collection in Modern-Era Retrospective analysis for Research and Applications version 2 (MERRA-2), with a spatial resolution of 0.5° × 0.625°. We downloaded the data of 2001–2025, and analyzed the annual variations of dust storms in northwest China and conduct a multi-factor analysis.

The 10-m horizontal wind components (used to calculate the wind speed and direction), geopotential height, mean sea level pressure, total precipitation and soil moisture data were accessed through the "ERA5 hourly data on single levels from 1940 to present" data set (ERA5: https://cds.climate.copernicus.eu/). ERA5, produced by the European Center for Medium Range Weather Forecasts (ECMWF), is a global atmospheric reanalysis data set with a spatial resolution of 0.25° × 0.25°, and an hour temporal resolution (Hersbach et al., 2020). We downloaded these data for the winter and spring seasons to analyze the spatial-temporal variation of wind speed, precipitation, soil moisture, and mean sea level pressure, and to examine their correlation with PM_{10} concentrations.

The Normalized Difference Vegetation Index (NDVI) data were obtained from the monthly MODIS Terra Vegetation Indices 1 km product (MOD13A3: https://earthdata.nasa.gov/). This data set, part of the Moderate Resolution Imaging Spectroradiometer (MODIS) Terra Vegetation Indices Monthly (MOD13A3) Version 6.1, is a gridded Level 3 product with a spatial resolution of 1 kilometer, provided monthly in a sinusoidal projection. In generating this monthly product, the algorithm ingests all the MOD13A3 products that overlap the month and employs a weighted temporal average. We downloaded NDVI data to analyze its spatial-temporal variation, and to examine its correlation with PM_{10} concentrations.

The land use data used in this study was derived from Landsat satellite imagery provided by the National Aeronautics and Space Administration (NASA) and processed on the Google Earth Engine (GEE) cloud computing platform. The imagery has a spatial resolution of 30 meters. Based on this data, we generated land use type products for northwest China from 2001 to 2025, which were subsequently used to calculate and analyze the Human Activity Intensity (HAI).

CMIP6 data were obtained through the Earth System Grid Federation (ESGF). This study selected the SSP1-2.6, SSP2-4.5 and SSP5-8.5 scenarios and employed three models, EC-Earth3-CC, MPI-ESM1-2-LR, and CESM2, to project springtime PM_{10} concentrations from 2026 to 2100.

2.3 Analytical methods

All statistical tests were two-tailed with a significance level of α = 0.05. Prior to statistical analysis, the normality of each continuous variable was assessed using the Shapiro-Wilk test (P > 0.05 indicating normality). Variables that deviated from normality were analyzed using non-parametric methods (Spearman correlation), while variables conforming to normality

https://doi.org/10.5194/egusphere-2026-3940
Preprint. Discussion started: 28 July 2026

were analyzed using parametric methods (joinpoint regression, segmented linear regression, and F-test) where applicable. Time-series trend analyses were based on annual data from the specified periods: n = 25 for 2001–2025, and n = 10 for 2016–2025. For station-based analyses (Spearman correlation and segmented regression), data were pooled across 26 monitoring stations over the 2016–2025 period, yielding n = 260 station-year pairs.

Spearman correlation coefficient (r) was employed to investigate the relationships between PM_{10} concentrations in northwest China and wind speed, precipitation, soil moisture, NDVI. The calculation formula is as follows (Wan et al., 2024):

$$r = 1 - \frac{6\sum_{i=1}^{n} d_i^2}{n(n^2 - 1)} \quad (1)$$

where ρ is the Spearman correlation coefficient, d_i is the difference in ranks between each pair of data, n is the sample size.

Joinpoint regression was used to detect trend turning points in the spring wind speed series from 2001 to 2025 (Muggeo, 2003). The method fits two linear segments joined at an unknown breakpoint and selects the breakpoint that minimizes the model's residual sum of squares. The search for the optimal breakpoint was restricted to the period 2005–2019 to avoid edge effects. An F-test comparing the selected joinpoint model with a simple linear model (no breakpoint) was performed to assess the significance of the trend change, and P-values were adjusted for multiple comparisons across candidate breakpoints using the Benjamini-Hochberg false discovery rate method. Bootstrap resampling (1,000 iterations) was applied to estimate 95% confidence intervals for the breakpoint years. All analyses were conducted in Python (version 3.13) using the NumPy and SciPy libraries.

We identified the critical thresholds using segmented linear regression (Elder and Fong, 2019). For each driver (wind speed, soil moisture, NDVI, and preceding-year precipitation) and its corresponding dependent variable (PM_{10} concentration or dust storm days), the data were sorted in ascending order by the independent variable. All possible breakpoints were iteratively tested, excluding the first and last 15% of data points to ensure sufficient sample sizes on both sides of the breakpoint. At each candidate breakpoint, two separate linear regressions were fitted to the left and right segments, and the coefficient of determination (R^2) of the two-segment model was calculated. The optimal threshold was defined as the breakpoint that maximized the R^2. To quantify the uncertainty of the estimated thresholds, we performed bootstrap resampling with 1,000 iterations. For each bootstrap sample, the segmented regression procedure was repeated, and the 2.5th and 97.5th percentiles of the bootstrap threshold distribution were taken as the 95% confidence interval.

We employed Random Forest (RF) regression to quantify the relative contributions of six environmental factors (wind speed, precipitation, soil moisture, NDVI, PGI, and HAI) to DUCMASS (dust column mass density). RF is an ensemble learning method that builds multiple decision trees and averages their predictions. Feature importance was derived from the average decrease in node impurity across all trees. This approach effectively handles non-linear relationships and multicollinearity among predictors. All analyses were performed using Python's scikit-learn and SciPy libraries.

This paper calculated human activity intensity (HAI) based on land use types. The calculation formula is as follows (Xu et al., 2016):

$$\mathrm{HAI} = \frac{S_{\mathrm{CLE}}}{S} \times 100\% \quad (2)$$

https://doi.org/10.5194/egusphere-2026-3940
Preprint. Discussion started: 28 July 2026

$$S_{\mathrm{CLE}} = \sum_{n=1}^{m} (\mathrm{SL}_n \times \mathrm{CI}_n) \quad (3)$$

When HAI represents the terrestrial surface human activity intensity index; S_{CLE} denotes the equivalent area of impervious surfaces within the region; S is the total area of the region; SLn represents the area of the nth type of land use within the region; CIn is the construction land equivalent conversion coefficient for the nth type of land use within the region (Table S1); and m represents the number of land use types within the region.

3 Results and discussion

3.1 Intensification and southward shift of Mongolian cyclones

To clarify the large-scale atmospheric circulation responsible for the recent rebound of dust storm activity over Northwest China, we composite circulation anomalies during 2021–2025 against the climatological mean of 1981–2020 (Fig. 1A, B). A pronounced negative sea-level pressure anomaly (-0.66 hPa) was centered over Mongolia at 119.5°E, 46.0°N (Fig. 1A). A positive relative vorticity anomaly intensified from 3.18 × 10^{-5} s^{-1} (at 106.5°E, 48.8°N) to 11.90 × 10^{-5} s^{-1} (at 95.0°E, 44.5°N, Fig. 1B), indicating a southward-shifted and intensified Mongolian cyclone.

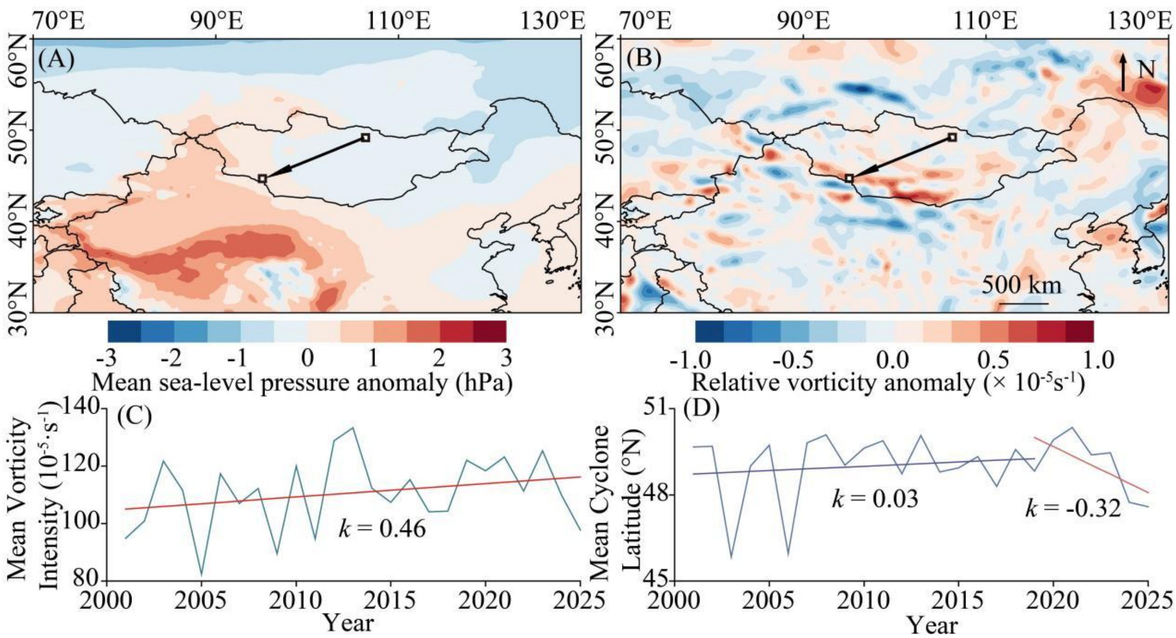

Fig. 1: (A) Sea level pressure anomalies from 2021–2025 compared to 1981–2020; (B) Vorticity anomalies from 2021–2025 compared 1981–2020; (C) The trend of changes of the mean vorticity intensity from 2001 to 2025; (D) The trend of changes of the mean cyclone latitude from 2001 to 2025.

Correspondingly, near-surface wind speeds rose by 0.32 m·s^{-1} across the Hexi Corridor and 0.63 m·s^{-1} over the Alxa Plateau for 2021–2025. These increments are 2–4 times greater than the marginal wind increase (+0.17 m·s^{-1}) in the Taklimakan Desert (Fig. S1A), highlighting a distinct spatial divergence in wind responses to cyclone activities. Such spatial disparity is

https://doi.org/10.5194/egusphere-2026-3940
Preprint. Discussion started: 28 July 2026

further modulated by regional prevailing wind regimes. The Taklimakan Desert is dominated by northeasterly winds, while northwesterly winds prevail over the Alxa Plateau and Hexi Corridor. As a result, the Alxa and Hexi regions are directly exposed to the strong northwesterly flows linked to Mongolian cyclones (Fig. S1B).

Long-term evolutionary trends of Mongolian cyclones from 2001 to 2025 provide solid evidence for the observed dust resurgence over Northwest China. The annual mean intensity of Mongolian cyclones increased from 94.84×10^{-5} s^{-1} to 97.76×10^{-5} s^{-1} throughout 2001–2025, revealing a persistent intensification of this synoptic system (Fig. 1C). The latitudinal position of the cyclone center remained nearly unchanged before 2020 (k = 0.03, P = 0.572), followed by an evident southward displacement after 2020 (approximately 2.08° latitude, Fig. 1D). Collectively, the combined effects of intensified intensity and southward migration of Mongolian cyclones are conducive to the development of extreme near-surface gales and long-range dust transport towards Northern China in the past five years.

The impacts of Mongolian cyclones on dust storms are strongly modulated by complex topographic features across Northern China. Encircled by the Tianshan and Kunlun Mountains, the Taklimakan Desert is dominated by northeasterly winds (Fig. S1B). Such topographic shielding largely weakens the influence of Mongolian cyclones on this region (Mu and Fiedler, 2025). Accordingly, local dust emissions and transport are primarily controlled by regional circulations (Zhu et al., 2025). On the contrary, the Alxa Plateau, Hexi Corridor and Mu Us Sandy Land are governed by persistent northwesterly winds. These areas lack large-scale mountain barriers and are highly vulnerable to the disturbances induced by Mongolian cyclones (Mu and Fiedler, 2025).

Interannual and decadal variations of Mongolian cyclone activity are also remotely forced by Arctic thermal anomalies. Rapid Arctic warming and declining sea ice concentration over the Barents Sea can perturb the structure and intensity of the polar vortex. This large-scale circulation perturbation generates anomalous circulations conducive to cyclogenesis over the Mongolia-Lake Baikal domain, ultimately increasing the frequency and strength of Mongolian cyclones and triggering frequent dust events across Northwest China (Wang et al., 2025a; Yin et al., 2022). In turn, radiative heating caused by suspended dust aerosols can reshape regional horizontal temperature gradients. This positive feedback further intensifies Mongolian cyclones and facilitates continuous dust emission and long-distance transport (Chen et al., 2023). To disentangle the relative contributions and nonlinear responses of multiple environmental drivers to dust activity, we subsequently explore the statistical relationships between PM_{10} concentrations and a suite of meteorological and land surface variables.

3.2 Reversal of dust activity after 2019 and spatial divergence

To quantify how dust activity responds to recent meteorological changes, we contrasted near-surface PM_{10} concentrations across two periods: 2016–2020 and 2021–2025 (Fig. S2A, B). Elevated PM_{10} levels exceeding 300 $\mu g \cdot m^{-3}$ were widely detected over the eastern Taklimakan Desert (Hotan, Hami and Aksu), the Hexi Corridor (Zhangye and Jiuquan) and the Alxa Plateau. After 2021, the number of monitoring stations recording PM_{10} within 300–500 $\mu g \cdot m^{-3}$ increased by 13 in the above regions. Meanwhile, stations with PM_{10} ranging from 200 to 300 $\mu g \cdot m^{-3}$ decreased by 174, primarily over the lower

https://doi.org/10.5194/egusphere-2026-3940
Preprint. Discussion started: 28 July 2026

Yellow River Basin, where PM_{10} concentrations declined to 100–200 $\mu g \cdot m^{-3}$. Such spatial disparities in aerosol loading are consistent with previous observational findings on East Asian dust distribution (Xing et al., 2025).

For targeted comparative analysis, we classified the entire study domain into four subregions: Source 1 (the Tarim Basin), Source 2 (the Alxa Plateau), dust transport pathways (areas adjacent to Source 2), and downwind urban areas (regions far away from primary dust sources; Fig. S1C, D). Distinct wind regimes exist across these subregions: the Tarim Basin is dominated by northeasterly winds, while northwesterly winds prevail over the remaining areas (Fig. S1B–D). Such wind field differences fundamentally determine the regional dust transport routes (Mu and Fiedler, 2025).

After 2021, the Tarim Basin (Source 1) experienced a 6.28% decline in PM_{10} concentrations. In contrast, notable rises were detected in Source 2 (+24.22%), transport pathways (+3.29%) and downwind cities (+17.68%; Fig. 2A; Fig. S3A–D). Spring dust column mass density (DUCMASS) derived from 2001–2025 datasets exhibited an evident trend reversal around 2019 (Fig. 2B), which synchronizes with the concurrent intensification and southward displacement of Mongolian cyclones (Luo et al., 2026) (Fig. 1A–D). During the period before 2019, DUCMASS increased at a rate of +0.006 $g \cdot m^{-2} \cdot yr^{-1}$ in the Tarim Basin, while it decreased at rates ranging from -0.005 to -0.004 $g \cdot m^{-2} \cdot yr^{-1}$ in other subregions. This pattern fully reversed after 2019: the Tarim Basin showed a decreasing trend (-0.013 $g \cdot m^{-2} \cdot yr^{-1}$), whereas Source 2, transport pathways and downwind areas all presented increasing trends with rates of +0.007, +0.002 and +0.003 $g \cdot m^{-2} \cdot yr^{-1}$, respectively (Table S2). Overall, the enhanced dust activities after 2019 are mainly limited to regions under the direct influence of Mongolian cyclones. By contrast, the topographically shielded Tarim Basin displays an opposite variation tendency, which further verifies the topographic modulation effect on dust evolution (Zhou et al., 2025b).

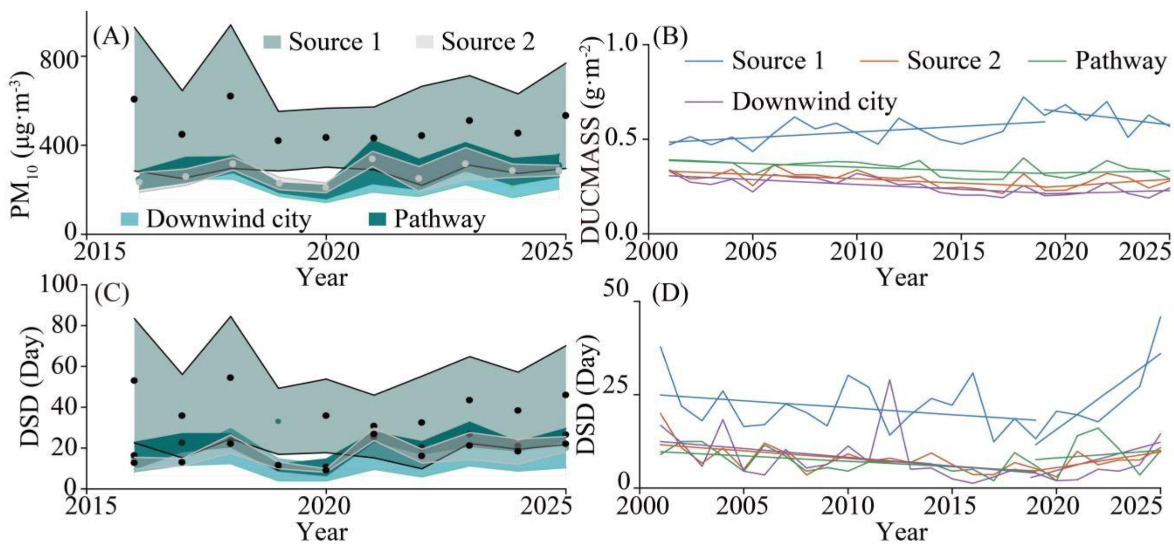

Fig. 2: (A) Interannual variations of near-surface PM_{10} concentrations during 2016–2025; (B) Interannual variations of spring dust column mass density (DUCMASS) from 2001 to 2025; (C) Mean dust storm days (DSD) across the four subregions derived from ground-based PM_{10} observations (2001–2025); (D) Mean DSD across the four subregions retrieved from NOAA datasets (2001–2025).

https://doi.org/10.5194/egusphere-2026-3940
Preprint. Discussion started: 28 July 2026

Ground-based PM_{10} observations for 2021–2025 reveal that compared with the 2016–2020 period, dust storm days (DSD) increased sharply in Source 2 (+49.68%), transport pathways (+42.54%) and downwind urban areas (+30.42%), while a decrease of -9.91% was observed over the Taklimakan Desert (Fig. 2C; Fig. S4A–D). DSD calculated from NOAA datasets also experienced a distinct trend reversal around 2019 (Fig. 2D). From 2001 to 2019, DSD presented a continuous decreasing trend across all four subregions, with decreasing rates ranging from -0.29 to -0.47 $d \cdot yr^{-1}$. After 2019, DSD turned to rise in all study areas. The most prominent increase occurred in Source 1 (+4.06 $d \cdot yr^{-1}$), followed by downwind urban areas (+1.51 $d \cdot yr^{-1}$), Source 2 (+0.84 $d \cdot yr^{-1}$) and transport pathways (+0.41 $d \cdot yr^{-1}$; Table S2). This discrepancy arises from different detection principles. NOAA DSD (visibility-based) captures elevated and weak dust layers, while DUCMASS reflects column-integrated loading. Over the Taklimakan, rising DSD but declining DUCMASS indicates more frequent but weaker dust events, a contrast most evident there.

3.3 Wind speed as the primary driver: threshold, trend, and cyclone linkage

Near-surface wind speed acts as the most direct dynamical bridge connecting Mongolian cyclone activities and regional dust emission. Compared with the 2016–2020 period, the 2021–2025 mean wind speed rose most remarkably over the Alxa Plateau (+0.63 $m \cdot s^{-1}$, +5.11%) and the Hexi Corridor (+0.32 $m \cdot s^{-1}$, +4.89%). In contrast, the Taklimakan Desert experienced only a marginal increase (+0.17 $m \cdot s^{-1}$, less than 2%; Fig. 3A; Fig. S2C, D). The interannual variation of March wind speed from 2001 to 2025 presents an obvious trend reversal around 2019 (Fig. 3B). From 2001 to 2019, wind speed declined steadily across all four subregions at rates ranging from -0.01 to -0.06 $m \cdot s^{-1} \cdot yr^{-1}$. After 2019, all trends flipped to positive, with increasing rates between +0.06 and +0.11 $m \cdot s^{-1} \cdot yr^{-1}$. This post-2019 wind recovery is most prominent over the Alxa Plateau (+0.11 $m \cdot s^{-1} \cdot yr^{-1}$), a region fully exposed to the influence of southward-displaced Mongolian cyclones (Table S2).

https://doi.org/10.5194/egusphere-2026-3940
Preprint. Discussion started: 28 July 2026

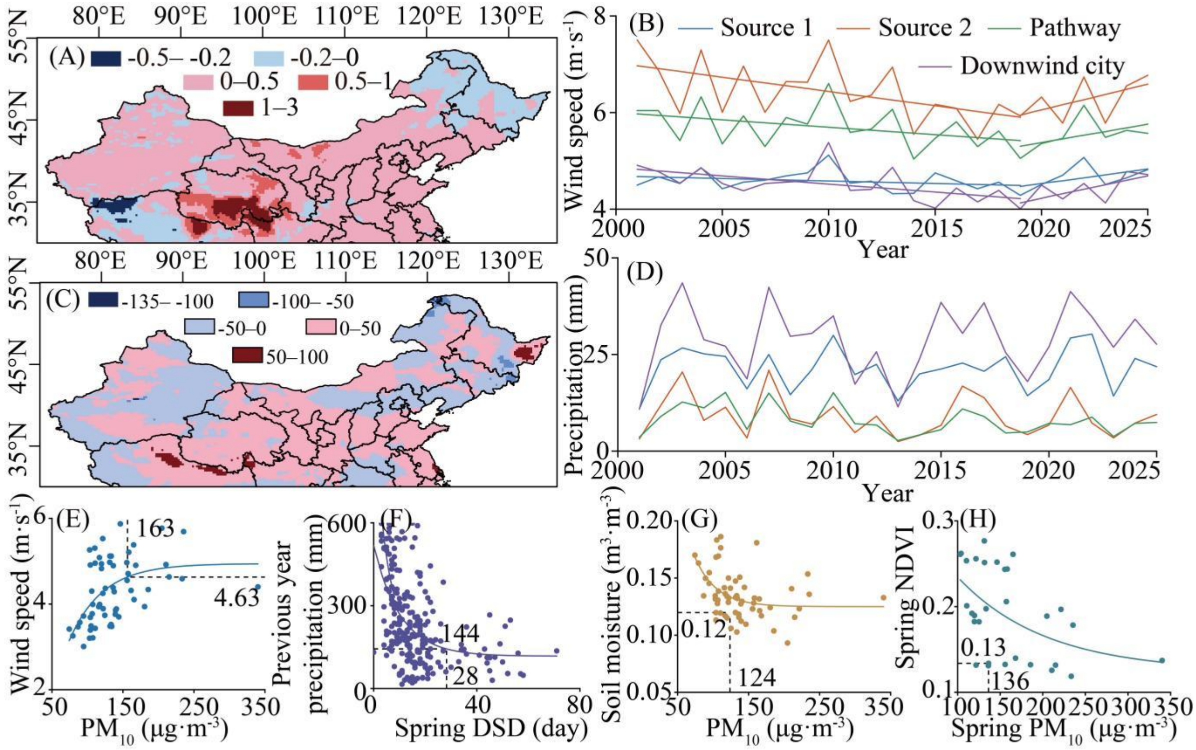

Fig. 3: (A) The difference of average wind speed between 2021–2025 and 2016–2020; (B) Interannual variations of wind speed from 2001 to 2025 March; (C) The difference of average precipitation between 2021–2025 and 2016–2020; (D) Interannual variations of precipitation from 2016 to 2025 March; (E) The index correlation graph of PM_{10} concentration and wind speed; (F) The index correlation graph of the DSD of spring and the precipitation of the previous year; (G) The index correlation graph of PM_{10} concentration and soil moisture; (H) The index correlation graph of PM_{10} concentration and NDVI in spring.

Wind speed acts as a critical mediator linking Mongolian cyclone activities to dust emission processes. Segmented linear regression reveals a critical wind speed threshold of 4.63 $m \cdot s^{-1}$ (95% confidence interval: 4.30–5.21 $m \cdot s^{-1}$; Fig. 3E). Once wind speed exceeds this threshold, near-surface PM_{10} concentrations rise drastically. The Spearman rank correlation coefficient between PM_{10} and wind speed is 0.49 ($P < 0.001$; Fig. S5A), confirming their significant positive correlation. The three most severe dust episodes during the study period (2021, 2023 and 2025) coincided with the highest spring wind speeds (4.45 ± 0.76 (s.d.), 4.49 ± 0.81 (s.d.), 4.61 ± 1.07 (s.d.) $m \cdot s^{-1}$; Fig. S6A–J) and the peak PM_{10} levels (149.3 ± 95.5 (s.d.), 345.9 ± 50.6 (s.d.), 374.2 ± 56.3 (s.d.) $\mu g \cdot m^{-3}$; Fig. 2A).

Wind speed is not simply a local meteorological variable, but a direct reflection of large-scale dynamical forcing induced by Mongolian cyclones. It dominates the entire lifecycle of dust particles, including emission, horizontal transport and dry deposition (Shao and Dong, 2006). Dust emission flux varies with wind speed following a cubic function, which is primarily controlled by saltation and abrasion processes over arid surfaces (Kok et al., 2012). Stronger near-surface winds lift saltating sand grains to greater heights and increase grain concentration, thereby substantially boosting dust aerosol emission (Kang et al., 2024). Regional topography also exerts remarkable modulation on surface wind fields (Fig. S1B). For instance, the Helan

Mountains deflect prevailing northwesterly flows and generate flank winds and lee vortices, which further reshape local dust mobilization and transport. On the spatial scale, persistent northwesterlies carry dust aerosols from the Taklimakan Desert and Alxa Plateau toward downstream areas. The correlation coefficient between PM_{10} and wind speed reaches 0.49 ($P \leq 0.001$) over the southwestern Taklimakan Desert, Alxa Plateau and Hexi Corridor (Fig. S5A), demonstrating that wind field variation serves as the dominant controller of dust storm activities across these key source regions.

3.4 Secondary modulators: precipitation, soil moisture, and vegetation

Although near-surface wind serves as the dominant dynamical driver for dust emission, precipitation, soil moisture and vegetation can effectively regulate surface soil erodibility and further modulate regional dust activities. In this section, we explore their statistical correlations with PM_{10} concentrations and examine their long-term evolutionary trends, aiming to clarify their roles in the dust resurgence after 2019.

The mean winter-to-spring precipitation across the study area was merely 12.4–12.6 mm during 2016–2025 (Fig. 3C; Fig. S2E, F). Meanwhile, March precipitation exhibited no statistically significant trend throughout 2001–2025 (Fig. 3D). A significant negative exponential relationship was detected between annual precipitation in the preceding year and spring dust storm days (DSD), with an effective suppression threshold of 143 mm (95% confidence interval: 112–212 mm; r = -0.52, $P < 0.001$; Fig. 3F). Nevertheless, annual precipitation over major dust sources is far lower than this critical value: less than 50 mm in the Taklimakan Desert and 100–150 mm across the Alxa Plateau. Accordingly, the direct inhibition of spring dust emission by contemporary precipitation remains limited (Fig. S5B). The lagged impact of antecedent precipitation, which acts via deep soil water recharge and sustained vegetation growth, is statistically significant but only exerts a minor influence on the interannual fluctuation of dust events.

Regional mean soil moisture across Northwest China was 0.14 ± 0.09 (s.d.) $m^3 \cdot m^{-3}$ for 2016–2025, and it declined slightly to 0.13 ± 0.09 (s.d.) $m^3 \cdot m^{-3}$ during 2021–2025 (Fig. 4A; Fig. S3G, H). From 2001 to 2025, March soil moisture presented a pronounced decreasing trend in all four subregions. The most remarkable declines occurred in Source 1 and the dust transport pathway, with rates of -0.0009 and -0.0008 $m^3 \cdot m^{-3} \cdot decade^{-1}$ (P = 0.003 and 0.006 respectively; Fig. 4B; Table S2). Soil moisture also follows a negative exponential relationship with PM_{10} concentrations, with an effective suppression threshold of 0.12 $m^3 \cdot m^{-3}$ (95% confidence interval: 0.12–0.15 $m^3 \cdot m^{-3}$; r = -0.36, P = 0.005; Fig. 3G; Fig. S5C). This value is considerably higher than the field-observed threshold for sand saltation initiation (Yang et al., 2020) (0.025 $m^3 \cdot m^{-3}$). Such discrepancy can be explained by three factors: the vertical mismatch between the ERA5 0–7 cm soil layer and the surface active layer, the spatial smoothing effect of reanalysis data versus in-situ point observations, and the essential difference between the dust suppression threshold and the saltation onset threshold.

https://doi.org/10.5194/egusphere-2026-3940
Preprint. Discussion started: 28 July 2026

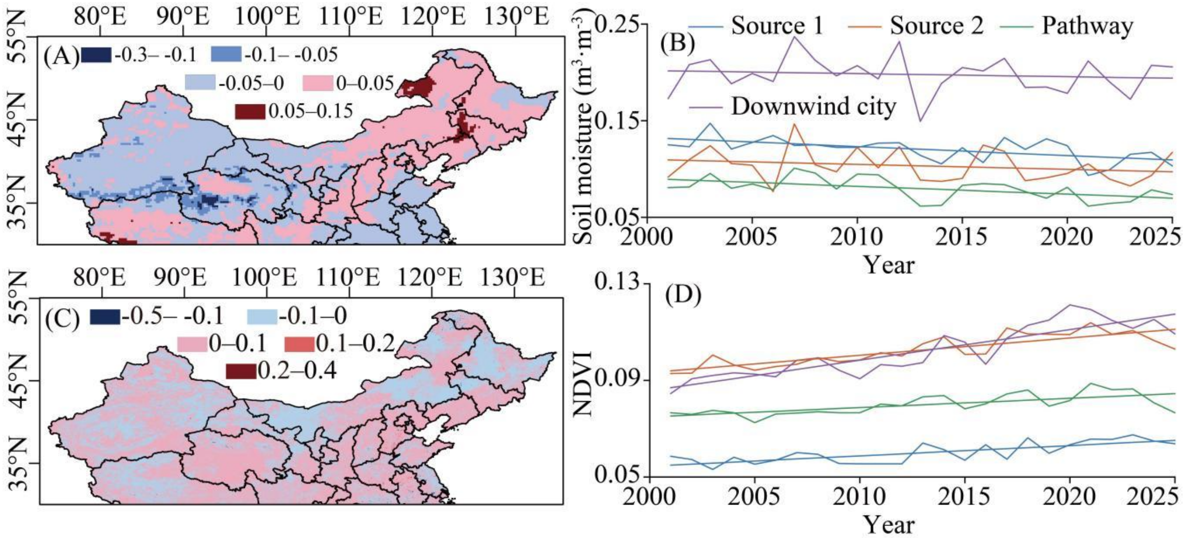

Fig. 4: (A) Differences in mean soil moisture between 2021–2025 and 2016–2020; (B) Interannual variations of March soil moisture (2001–2025); (C) Differences in mean NDVI between 2021–2025 and 2016–2020; (D) Interannual variations of March NDVI (2001–2025).

Spring normalized difference vegetation index (NDVI) shows a significant negative correlation with PM_{10} concentrations (r = -0.51, P = 0.009), with an effective dust suppression threshold of 0.13 (95% confidence interval: 0.13–0.19; Fig. 3H; Fig. S5D). The regional mean vegetation coverage across Northwest China increased mildly from 0.16 ± 0.08 (s.d.) (2016–2020) to 0.17 ± 0.08 (s.d.) (2021–2025; Fig. 4C; Fig. S3I, J). During 2001–2025, March NDVI exhibited significant rising trends across all subregions: +0.04 decade^{-1} for Source 1, +0.07 decade^{-1} for Source 2, +0.04 decade^{-1} for the Hexi Corridor, and +0.13 decade^{-1} for downwind urban areas (all $P \leq 0.001$; Fig. 4D; Table S2). Such widespread vegetation greening is primarily attributed to artificial afforestation rather than climatic change, given the stable winter-to-spring precipitation (Zhou et al., 2025a). Nevertheless, March NDVI values over major dust sources, ranging from 0.05 to 0.07 in the Taklimakan Desert, are consistently lower than the 0.13 threshold. As a result, sparse vegetation cannot provide effective dust inhibition (Fig. 3H; Fig. 4D). Two additional factors further weaken the vegetation suppression effect: the seasonal mismatch that NDVI reaches its minimum in March (the peak dust season), and the limited capability of satellite products to capture non-photosynthetic vegetation such as dry grass and litter (Chappell et al., 2023). Overall, vegetation greening has alleviated dust pollution to a certain extent, yet it fails to offset the wind-induced dust enhancement.

Precipitation inhibits dust activity indirectly via obvious time lags, mainly by elevating soil moisture and promoting vegetation growth (Kang et al., 2024). Elevated soil moisture strengthens soil particle cohesion and facilitates soil crust development, which consequently increases the threshold wind velocity for wind erosion (Fécan et al., 1999; Yang et al., 2020). Vegetation cover restrains dust emission through three pathways: canopy interception of airborne particles, increased surface roughness, and soil consolidation by plant roots (Liu et al., 2004, 2020). Since antecedent precipitation replenishes deep soil water and maintains vegetation vitality into the following spring, dust storm days correlate more closely with

https://doi.org/10.5194/egusphere-2026-3940
Preprint. Discussion started: 28 July 2026

preceding-year precipitation than with concurrent rainfall (Gong et al., 2024) (r = -0.52, P < 0.001). Despite the potential overestimation of dust suppression derived from the 0–7 cm ERA5 soil moisture dataset, caused by vertical deviation from the actual surface active layer (Okin, 2022), the threshold value of 0.12 $m^3 \cdot m^{-3}$ determined in this study can serve as a reliable quantitative benchmark for dust control across Northwest China.

NDVI was positively correlated with Human Activity Intensity (HAI, r = 0.49, P = 0.014), whereas its negative relationship with PM_{10} became stronger after controlling for precipitation and soil moisture (partial r = -0.62, P < 0.001). These results suggest that vegetation greening in northwest China is not solely driven by hydroclimatic variability and is likely associated with ecological restoration and land management activities. Vegetation mitigates dust emission via canopy interception, increased surface roughness and root-induced soil consolidation (Liu et al., 2020; Zhou et al., 2025a). After decades of ecological restoration, spring NDVI over key dust sources such as the Taklimakan Desert still ranges only from 0.05 to 0.07, which is far below the effective suppression threshold of 0.13 (Fig. 3H, Fig. 4D). In the meantime, the intensified and southward-displaced Mongolian cyclone has greatly strengthened near-surface winds, especially over downwind regions including the Alxa Plateau and Hexi Corridor. Such strong wind forcing overwhelms the weak inhibitory effects of existing vegetation and soil moisture (Fig. 1A–D). Accordingly, large-scale ecological projects such as the Three-North Shelterbelt Program need to be further promoted, with priority given to areas where NDVI values are below the effective dust suppression threshold.

3.5 Pathways and future impacts of Mongolian cyclone forcing on dust activity

To quantify the pathways through which Mongolian cyclone anomalies affect dust activity, a random forest model was used to evaluate the relative importance of meteorological and land-surface factors that are directly or indirectly linked to cyclone variability (Fig. S7A). In the Taklimakan Desert (R^2 = 0.87), wind speed was the dominant factor (0.67; Fig. 5A). In the Alxa Plateau (R^2 = 0.83; Fig. 5B) and Mu Us Sandy Land (R^2 = 0.79; Fig. 5C), wind speed remained dominant (0.66 and 0.64). Compared with the Taklimakan Desert, the contributions of precipitation and Pressure Gradient Index (PGI) were substantially larger in the Alxa Plateau and Mu Us Sandy Land (precipitation: 0.03 and 0.22 and 0.22; PGI: 0.03, 0.08 and 0.06), while NDVI contributed less (0.23, 0.03 and 0.04). Soil moisture showed minimal regional variation (0.04, 0.02 and 0.03). In the surrounding urban areas (Taklimakan: R^2 = 0.77, Fig. S7B; Alxa: R^2 = 0.78, Fig. S7C; Mu Us: R^2 = 0.67, Fig. S7D), HAI was introduced. In the Taklimakan periphery, wind speed and PGI remained largely unchanged (0.59 and 0.09). In the Alxa and Mu Us peripheries, wind speed decreased markedly (both 0.25), while PGI increased significantly (0.37 and 0.38). Precipitation, soil moisture, and NDVI showed minor changes, and HAI contributed the least (0.07–0.10).

https://doi.org/10.5194/egusphere-2026-3940
Preprint. Discussion started: 28 July 2026

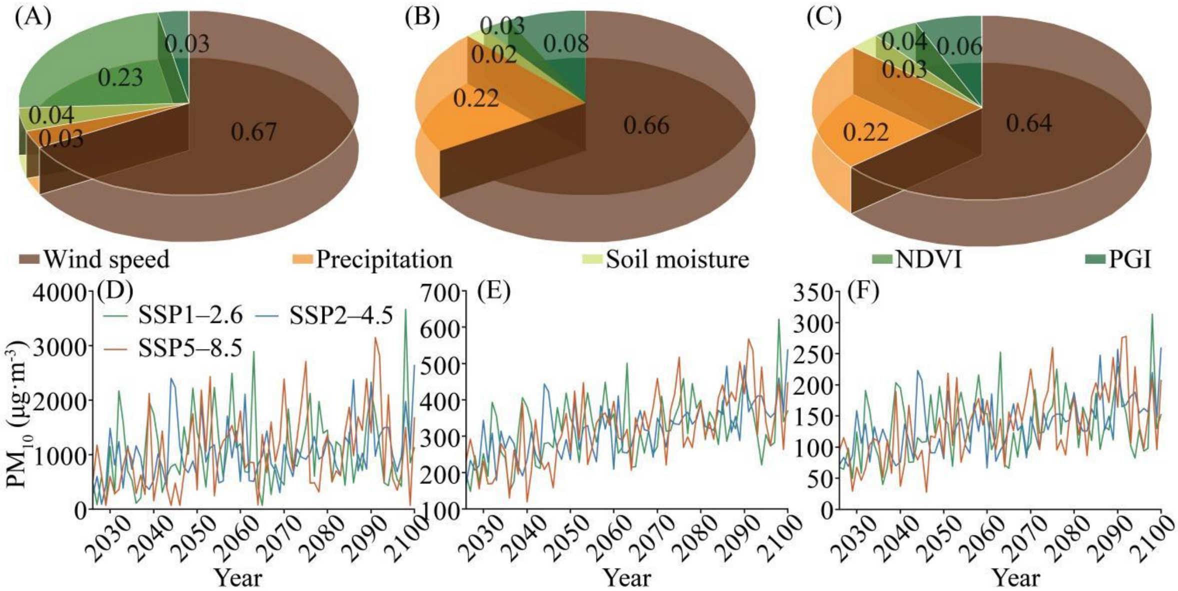

Fig. 5: (A–C) Relative contributions of various factors to PM_{10} concentrations in the Taklimakan Desert, Alxa Plateau, and Mu Us Sandy Land, respectively. (D–F) Predicted future PM_{10} concentrations in cities surrounding the Taklimakan Desert, Alxa Plateau, and Mu Us Sandy Land, respectively.

Wind speed is the primary dust driver through dynamical forcing by the enhanced southward-shifted Mongolian cyclone, while precipitation, soil moisture, and vegetation act as secondary pathways. Despite no significant precipitation trend, increased wind speed, decreased soil moisture, and vegetation below the 0.13 threshold jointly raised dust storm days with spatial heterogeneity (Fig. 3B, D; Fig. 4B, D). Precipitation contributed only 3% in the hyper-arid Taklimakan, where NDVI played a relatively important role (Aili et al., 2023). In contrast, precipitation contributed 22% in Alxa and Mu Us, where stronger cyclone influence weakened NDVI's independent effect (Elshora et al., 2024; Xie et al., 2025). In urban areas, wind contribution declined while PGI rose, indicating enhanced regional transport. These factors interact via land-atmosphere coupling (Filonchyk et al., 2024; Zhou et al., 2024), but seasonal decoupling between wind and rain limits mitigation, sustaining dry-season dust storms (Okin, 2022; Tan et al., 2025).

Based on historical data, CMIP6 future scenarios (SSP1-2.6, SSP2-4.5, SSP5-8.5) were used to project PM_{10} concentrations for 2026–2100 (Fig. 5D–F). The results indicate an increasing trend in all three regions, with the largest increase in the Taklimakan Desert (231.6%–241.0%, Fig. 5D), followed by the Alxa Plateau (134.8%–135.3%, Fig. 5E), and the smallest increase in the Mu Us Sandy Land (27.0%–28.4%, Fig. 5F). These differences are mainly associated with vegetation changes, as vegetation cover increases by 18.34% in the Alxa Plateau and 39.64% in the Mu Us Sandy Land, partially mitigating the rise in PM_{10}. Under different emission scenarios, PM_{10} under SSP5-8.5 is slightly higher than under SSP1-2.6 and SSP2-4.5, but the differences are small (<3%), indicating that PM_{10} in northwestern China is relatively low sensitivity to emission pathways and is primarily controlled by climate-driven increases in wind speed and soil drying.

https://doi.org/10.5194/egusphere-2026-3940
Preprint. Discussion started: 28 July 2026

Our results differ from Zhao et al. (Zhao et al., 2023), who projected a future decline in dust activity (0.8%–11.9%), mainly due to differences in seasonal focus and the influence of the Mongolian cyclone. While Zhao et al. (Zhao et al., 2023) analyzed annual mean changes, our study focuses on spring, the peak dust season, and reveals increasing wind speeds that are masked in annual averages. Spring wind speed increased by 33.08% in the Taklimakan Desert and 15.61% in the Alxa Plateau. Although vegetation increases in the Alxa Plateau and Mu Us Sandy Land partly mitigate PM_{10} growth (Fu et al., 2026), PM_{10} in northwest China remains weakly sensitive to emission pathways and is primarily controlled by climate-driven strengthening of Mongolian cyclone activity, which enhances wind forcing and surface drying. As wind speed is the dominant driver of dust activity, the projected PM_{10} increase likely reflects stronger cyclone-related atmospheric forcing. This highlights the Mongolian cyclone as a key large-scale driver of future dust activity in northwest China, supporting the view that future dust trends are governed primarily by climate dynamics rather than emission pathways (Gan et al., 2026).

Based on the above results, a conceptual framework was developed to summarize the influence pathways of Mongolian cyclone intensification on dust activity in northwest China (Fig. 6).

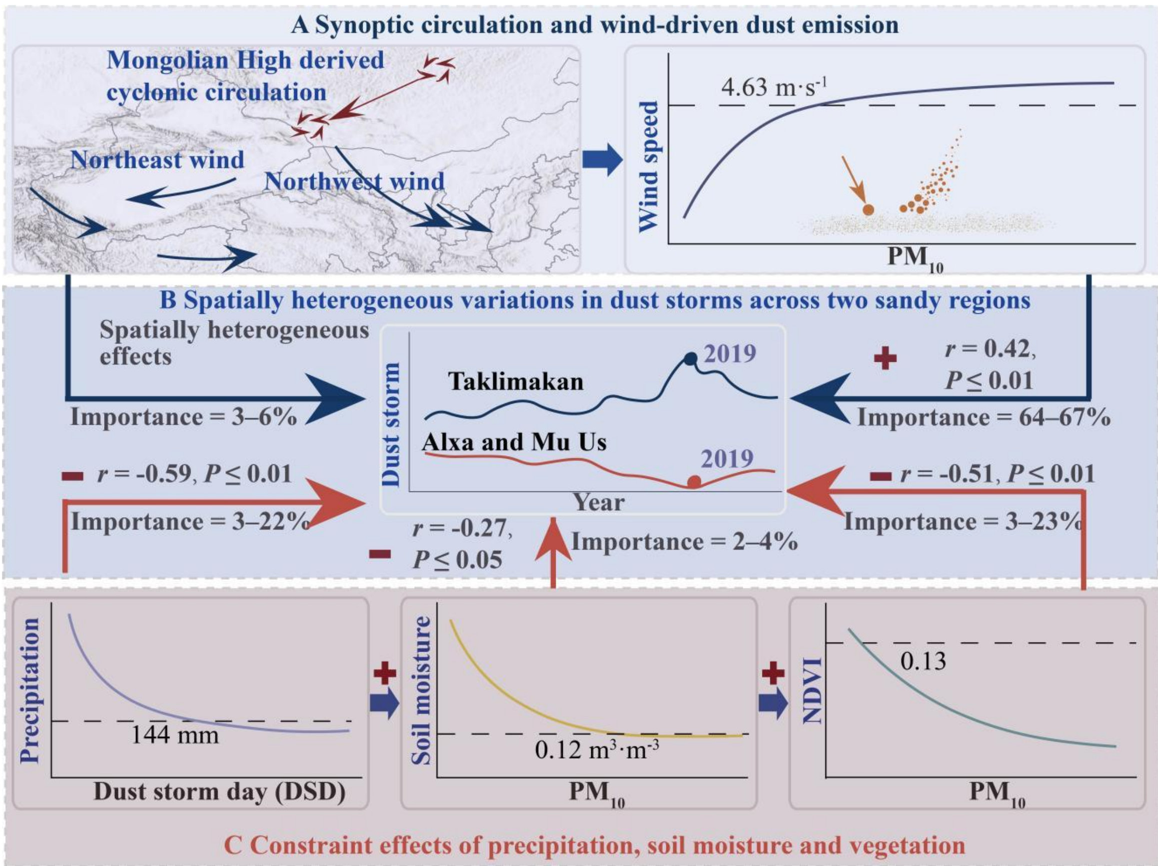

Fig. 6: Schematic diagram illustrating the mechanisms linking intensified Mongolian cyclones to dust storm activities over Northwest China ("+" represents promotion, and "-" represents inhibition).

4 Conclusion

This study quantifies the intensification and southward shift of Mongolian cyclones since 2001 and explains their spatially divergent impacts on dust activity across northwest China. Using multi-source observational data, random forest modeling, and CMIP6 projections, we demonstrate that cyclone intensity increased from 94.84×10^{-5} s^{-1} to 97.76×10^{-5} s^{-1} with a southward displacement of 2.08° after 2019. Correspondingly, spring near surface wind speed (+17.38%) and DUCMASS (+9.85%) rose markedly after 2019 in regions except the Taklimakan Desert, where wind speed increased by only 6.03% and DUCMASS declined by 9.27%. Wind speed was the dominant control on dust activity (contribution > 0.60) with an emission threshold of 4.63 $m \cdot s^{-1}$; precipitation, soil moisture, and NDVI acted as secondary modulators with suppression thresholds of 144 mm, 0.12 $m^3 \cdot m^{-3}$, and 0.13, respectively. CMIP6 projects rising PM_{10} through 2100, with < 3% difference across emission scenarios.

The divergent responses are primarily governed by regional wind regimes. Regions such as the Alxa Plateau and the Hexi Corridor, where northwesterly winds prevail, are more directly affected by cyclone forcing, whereas the Taklimakan Desert is characterized by northeasterly winds and topographic shielding, resulting in dust activity being more strongly influenced by local thermally driven circulations. This spatial heterogeneity demonstrates that the influence of Mongolian cyclones depends not only on cyclone intensity but also on the coupling between large-scale circulation, regional wind regimes, and topographic constraints.

Previous studies have mainly attributed the long-term decline in dust activity over northern China to weakened winds, vegetation recovery, and other land-surface changes, while the Taklimakan Desert has often been regarded as the dominant dust source. Our results indicate that these mechanisms alone cannot explain the post-2019 dust resurgence. Consistent with our random forest attribution, wind speed explained more than 60% of the variance in dust activity, whereas land-surface factors acted primarily as secondary modulators. Together, these results demonstrate that intensified Mongolian cyclones represent the primary large-scale driver, whereas regional wind regimes and topographic constraints determine the magnitude and even the direction of regional dust responses. By quantifying both the atmospheric forcing and the corresponding emission thresholds, this study extends previous understanding of East Asian dust dynamics from qualitative attribution toward process-based regional differentiation.

These findings provide new insight into the mechanisms controlling the atmospheric dust cycle under a changing climate. They indicate that changes in large-scale atmospheric circulation may outweigh gradual land-surface changes in regulating recent dust variability over East Asia. Consequently, Earth system and aerosol models should explicitly represent cyclone-topography-wind interactions to improve simulations of dust emission, transport, radiative forcing, and dust-climate feedbacks. The strong regional heterogeneity identified here also suggests that future dust mitigation and ecosystem management should adopt region-specific rather than uniform strategies.

Although this study improves understanding of how intensified Mongolian cyclones influence dust activity, several limitations remain, including the relatively short 2001–2025 record, the lack of numerical validation of the proposed mechanism, and uncertainties in ERA5 soil moisture. Future coupled climate-dust modeling is needed to further test causality and seasonal cyclone-dust interactions. Nevertheless, the consistency among multiple observational datasets, machine-learning attribution, and CMIP6 projections increases confidence in the robustness of the proposed mechanism.

Overall, this study demonstrates that intensified Mongolian cyclones have emerged as a key regulator of recent dust variability over northwestern China and highlights the importance of explicitly representing circulation-topography interactions in future Earth system and aerosol models.

Code and data availability

The PM_{10} concentration data used in this study are available from the China National Environment Monitoring Centre (CNEMC): https://www.cnemc.cn/. The ERA5 reanalysis data (Hersbach et al., 2020) are available from the Copernicus Climate Change Service: https://doi.org/10.24381/cds.adbb2d47. The MERRA-2 aerosol data (Global Modeling and Assimilation Office and Pawson, 2015) are available from NASA GES DISC: https://doi.org/10.5067/0JRLVL8YV2Y4. The MODIS NDVI data (Didan, 2015) are available from NASA Earthdata: https://doi.org/10.5067/MODIS/MOD13A3.061. The CMIP6 model output used for future projections is available from the Earth System Grid Federation (ESGF): https://esgf-node.llnl.gov/search/cmip6/. All other data used in this study are available from the corresponding author upon reasonable request.

Author contributions

Z.W.H. and Z.Z.C. conceived and designed the study. Z.W.H., Z.L.G., and Z.Z.Y. performed the data curation and formal analysis. Z.W.H., L.Y.Z., and W.S.Q. conducted the methodology and validation. Z.W.H. wrote the original draft. Z.Z.C., F.P., D.Z.B., W.W.S., and Y.L.M. reviewed and edited the manuscript. Z.Z.C. acquired the funding and provided project administration. All authors read and approved the final manuscript.

Competing interests

The authors declare no competing interests.

Acknowledgements

We are grateful for the financial assistance obtained from the major program of Inner Monglia (2024JBGS0003-1-1), the Inner Mongolia Academy of Forestry Sciences Open Research Project (KF2025ZD07), the Fundamental Research Funds for the Central Universities (GK202502004, GK202306002, GK202309006), Science & Technology Fundamental Resources

Investigation Program (2022FY202304), and from the Natural Science Basic Research Program of Shaanxi (2023-JC-QN-0301). We thank the journal's anonymous reviewers for their efforts to improve our manuscript.

References

Aili, A., Xu, H., Xu, Q., and Liu, K.: Aeolian dust movement and deposition under local atmospheric circulation in a desert-oasis transition zone of the northeastern Taklimakan desert, Ecological Indicators, 157, 111289, https://doi.org/10.1016/j.ecolind.2023.111289, 2023.

An, L., Che, H., Xue, M., Zhang, T., Wang, H., Wang, Y., Zhou, C., Zhao, H., Gui, K., Zheng, Y., Sun, T., Liang, Y., Sun, E., Zhang, H., and Zhang, X.: Temporal and spatial variations in sand and dust storm events in East Asia from 2007 to 2016: Relationships with surface conditions and climate change, Science of The Total Environment, 633, 452–462, https://doi.org/10.1016/j.scitotenv.2018.03.068, 2018.

Bishop, J. K. B., Davis, R. E., and Sherman, J. T.: Robotic Observations of Dust Storm Enhancement of Carbon Biomass in the North Pacific, Science, 298, 817–821, https://doi.org/10.1126/science.1074961, 2002.

Chappell, A., Webb, N. P., Hennen, M., Zender, C. S., Ciais, P., Schepanski, K., Edwards, B. L., Ziegler, N. P., Balkanski, Y., Tong, D., Leys, J. F., Heidenreich, S., Hynes, R., Fuchs, D., Zeng, Z., Baddock, M. C., Lee, J. A., and Kandakji, T.: Elucidating Hidden and Enduring Weaknesses in Dust Emission Modeling, JGR Atmospheres, 128, e2023JD038584, https://doi.org/10.1029/2023JD038584, 2023.

Chen, Y., Chen, S., Zhou, J., Zhao, D., Bi, H., Zhang, Y., Alam, K., Yu, H., Yang, Y., and Chen, J.: A super dust storm enhanced by radiative feedback, npj Clim Atmos Sci, 6, 90, https://doi.org/10.1038/s41612-023-00418-y, 2023.

Didan, K.: MOD13A3 MODIS/Terra vegetation Indices Monthly L3 Global 1km SIN Grid V061, https://doi.org/10.5067/MODIS/MOD13A3.061, 2021.

Elder, A. and Fong, Y.: Estimation and inference for upper hinge regression models, Environ Ecol Stat, 26, 287–302, https://doi.org/10.1007/s10651-019-00428-1, 2019.

Elshora, M., Xia, H., Su, L., and Wei, T.: Observation and study of consecutive dust storms in the Taklimakan desert from March 16 to 27, 2022, using reanalysis models and lidar, Atmospheric Research, 305, 107431, https://doi.org/10.1016/j.atmosres.2024.107431, 2024.

Engelstaedter, S., Kohfeld, K. E., Tegen, I., and Harrison, S. P.: Controls of dust emissions by vegetation and topographic depressions: An evaluation using dust storm frequency data, Geophysical Research Letters, 30, 2002GL016471, https://doi.org/10.1029/2002GL016471, 2003.

Falkowski, P. G., Barber, R. T., and Smetacek, V.: Biogeochemical Controls and Feedbacks on Ocean Primary Production, Science, 281, 200–206, https://doi.org/10.1126/science.281.5374.200, 1998.

Fécan, F., Marticorena, B., and Bergametti, G.: Parametrization of the increase of the aeolian erosion threshold wind friction velocity due to soil moisture for arid and semi-arid areas, Ann. Geophys., 17, 149–157, https://doi.org/10.1007/s00585-999-0149-7, 1999.

Filonchyk, M.: Characteristics of the severe March 2021 Gobi Desert dust storm and its impact on air pollution in China, Chemosphere, 287, 132219, https://doi.org/10.1016/j.chemosphere.2021.132219, 2022.

Filonchyk, M., Peterson, M. P., Zhang, L., and Yan, H.: An analysis of air pollution associated with the 2023 sand and dust storms over China: Aerosol properties and PM10 variability, Geoscience Frontiers, 15, 101762, https://doi.org/10.1016/j.gsf.2023.101762, 2024.

Fu, Y., Wu, C., Gao, S., Peñuelas, J., Camarero, J. J., Zhang, J., Li, D., Zheng, X., Li, Z., Wang, Y., Liang, E., and Piao, S.: Vegetation greening drives long-term dust mitigation in Eastern Asia, Nat Commun, 17, 1729, https://doi.org/10.1038/s41467-026-68427-y, 2026.

Gan, Y., Zhang, Z., Chu, W., Ding, J., and Ren, Y.: Assessment and prediction of dust emissions, deposition and radiation forcing in Central Asia, Atmos. Chem. Phys., 26, 3881–3900, https://doi.org/10.5194/acp-26-3881-2026, 2026.

Gao, J., Ding, T., and Gao, H.: Dominant circulation pattern and moving path of the Mongolian Cyclone for the severe sand and dust storm in China, Atmos. Res., 301, 107272, https://doi.org/10.1016/j.atmosres.2024.107272, 2024.

Global Modeling and Assimilation Office and Pawson, S.: MERRA-2 tavgM_2d_flx_Nx: 2d,Monthly mean,Time-Averaged,Single-Level,Assimilation,Surface Flux Diagnostics V5.12.4, https://doi.org/10.5067/0JRLVL8YV2Y4, 2015.

Gong, H., Wang, G., Fan, C., Zhuo, X., Sha, L., Kuang, Z., Bi, J., and Cheng, T.: Temporal accumulation and lag effects of precipitation on carbon fluxes in terrestrial ecosystems across semi-arid regions in China, Agricultural and Forest Meteorology, 356, 110189, https://doi.org/10.1016/j.agrformet.2024.110189, 2024.

Goudie, A. S.: Desert dust and human health disorders, Environment International, 63, 101–113, https://doi.org/10.1016/j.envint.2013.10.011, 2014.

Han, L., Zhang, Z., Liang, A., Lu, J., Dong, Z., and Zhang, Z.: Deciphering dust provenance and transport pathways across Northern China's source-sink systems, Atmos. Chem. Phys., 25, 15343–15357, https://doi.org/10.5194/acp-25-15343-2025, 2025.

Hersbach, H., Bell, B., Berrisford, P., Hirahara, S., Horányi, A., Muñoz‐Sabater, J., Nicolas, J., Peubey, C., Radu, R., Schepers, D., Simmons, A., Soci, C., Abdalla, S., Abellan, X., Balsamo, G., Bechtold, P., Biavati, G., Bidlot, J., Bonavita, M., De Chiara, G., Dahlgren, P., Dee, D., Diamantakis, M., Dragani, R., Flemming, J., Forbes, R., Fuentes, M., Geer, A., Haimberger, L., Healy, S., Hogan, R. J., Hólm, E., Janisková, M., Keeley, S., Laloyaux, P., Lopez, P., Lupu, C., Radnoti, G., De Rosnay, P., Rozum, I., Vamborg, F., Villaume, S., and Thépaut, J.: The ERA5 global reanalysis, Quart J Royal Meteoro Soc, 146, 1999–2049, https://doi.org/10.1002/qj.3803, 2020.

Hu, Z., Ma, Y., Jin, Q., Idrissa, N. F., Huang, J., and Dong, W.: Attribution of the March 2021 exceptional dust storm in North China, Bulletin of the American Meteorological Society, 104, E749–E755, https://doi.org/10.1175/BAMS-D-22-0151.1, 2023.

Kang, H., Zhu, B., De Leeuw, G., Van Der A, R. J., Lu, W., Shen, X., and Guo, Z.: Source contributions to two super dust storms over Northern China in March 2021 and the impact of soil moisture, Science of The Total Environment, 950, 175289, https://doi.org/10.1016/j.scitotenv.2024.175289, 2024.

Kok, J. F., Parteli, E. J. R., Michaels, T. I., and Karam, D. B.: The physics of wind-blown sand and dust, Rep. Prog. Phys., 75, 106901, https://doi.org/10.1088/0034-4885/75/10/106901, 2012.

Li, H. and Wang, C.: Impact of dust radiation effect on simulations of temperature and wind – A case study in Taklimakan Desert, Atmospheric Research, 273, 106163, https://doi.org/10.1016/j.atmosres.2022.106163, 2022.

Liu, X., Yin, Z., Zhang, X., and Yang, X.: Analyses of the spring dust storm frequency of northern China in relation to antecedent and concurrent wind, precipitation, vegetation, and soil moisture conditions, J. Geophys. Res., 109, 2004JD004615, https://doi.org/10.1029/2004JD004615, 2004.

Liu, X., Min, R., Zhang, H., Wang, Q., and Song, H.: Land cover changes reduce dust aerosol concentrations in Northern China (2000–2020), Environmental Research, 268, 120823, https://doi.org/10.1016/j.envres.2025.120823, 2025.

Liu, Y., Wang, G., Hu, Z., Shi, P., Lyu, Y., Zhang, G., Gu, Y., Liu, Y., Hong, C., Guo, L., Hu, X., Yang, Y., Zhang, X., Zheng, H., and Liu, L.: Dust storm susceptibility on different land surface types in arid and semiarid regions of northern China, Atmospheric Research, 243, 105031, https://doi.org/10.1016/j.atmosres.2020.105031, 2020.

Luo, N., Ding, R., Meng, M., and Wang, W.: Drivers to recent springtime dust activity in East Asia, Global and Planetary Change, 256, 105184, https://doi.org/10.1016/j.gloplacha.2025.105184, 2026.

Mu, F. and Fiedler, S.: How much do atmospheric depressions and Mongolian cyclones contribute to spring dust activities in East Asia?, npj Clim Atmos Sci, 8, 51, https://doi.org/10.1038/s41612-025-00929-w, 2025.

Muggeo, V. M. R.: Estimating regression models with unknown break - points, Statistics in Medicine, 22, 3055–3071, https://doi.org/10.1002/sim.1545, 2003.

Okin, G. S.: Where and How Often Does Rain Prevent Dust Emission?, Geophysical Research Letters, 49, e2021GL095501, https://doi.org/10.1029/2021GL095501, 2022.

Pu, B. and Jin, Q.: A Record-Breaking Trans-Atlantic African Dust Plume Associated with Atmospheric Circulation Extremes in June 2020, Bulletin of the American Meteorological Society, 102, E1340–E1356, https://doi.org/10.1175/BAMS-D-21-0014.1, 2021.

Shao, Y. and Dong, C. H.: A review on East Asian dust storm climate, modelling and monitoring, Global and Planetary Change, 52, 1–22, https://doi.org/10.1016/j.gloplacha.2006.02.011, 2006.

Tam, W. W. S., Wong, T. W., Wong, A. H. S., and Hui, D. S. C.: Effect of dust storm events on daily emergency admissions for respiratory diseases, Respirology, 17, 143–148, https://doi.org/10.1111/j.1440-1843.2011.02056.x, 2012.

Tan, C., Liu, C., Li, T., Liu, X., Tang, M., and Zhao, T.: Spatiotemporal Variations and Key Driving Factors of Dust Storms in China's Source Regions from 2000 to 2024, Atmosphere, 16, 589, https://doi.org/10.3390/atmos16050589, 2025.

Tong, D., Feng, I., Gill, T. E., Schepanski, K., and Wang, J.: How Many People Were Killed by Windblown Dust Events in the United States?, Bulletin of the American Meteorological Society, 104, E1067–E1084, https://doi.org/10.1175/BAMS-D-22-0186.1, 2023.

Victor, J. N., Potdar, S. S., Siingh, D., Gokul, T., Kamra, A. K., Singh, R. P., Gopalakrishnan, V., and Pandithurai, G.: Impact of a severe dust storm on aerosol properties and their radiative forcing over the Indian subcontinent during winter, Atmospheric Research, 301, 107282, https://doi.org/10.1016/j.atmosres.2024.107282, 2024.

Wan, Z., Yang, C., Wang, X., Xue, Y., Zhao, J., Cui, J., Guo, Q., Hua, H., Sun, H., Chen, D., Zhao, W., Xiao, Y., and Wang, W.: Spatial and temporal differentiation of air quality and its influence factors in 16 cities in Shandong Province from 2019 to 2020, RSC Sustainability, 2, 1528–1542, https://doi.org/10.1039/D4SU00128A, 2024.

Wang, J., Chen, L., and Li, S.: The Influence of North Atlantic Sea Surface Temperature and Sea Ice in the Barents Sea on Spring Mongolian Cyclone Activity, Journal of Climate, 38, 877–889, https://doi.org/10.1175/JCLI-D-24-0407.1, 2025a.

Wang, L., Hou, C., Pang, X., Zhang, H., Yizhaq, H., Mason, J. A., Lu, H., and Xu, Z.: Slowdown of Dune Migration in East Asia's Inland Deserts: A 35 - Year Response to Wind Stilling, Geophysical Research Letters, 52, e2024GL113506, https://doi.org/10.1029/2024GL113506, 2025b.

White, J. R., Balling, R. C., and Cerveny, R. S.: Topographic shielding and funneling for dust events associated with the North American Monsoon in the Sonoran Desert, central Arizona, USA, Journal of Arid Environments, 224, 105233, https://doi.org/10.1016/j.jaridenv.2024.105233, 2024.

Wu, C., Lin, Z., He, J., Zhang, M., Liu, X., Zhang, R., and Brown, H.: A process - oriented evaluation of dust emission parameterizations in CESM: Simulation of a typical severe dust storm in E ast A sia, J Adv Model Earth Syst, 8, 1432–1452, https://doi.org/10.1002/2016MS000723, 2016.

Wu, C., Lin, Z., Shao, Y., Liu, X., and Li, Y.: Drivers of recent decline in dust activity over East Asia, Nat Commun, 13, 7105, https://doi.org/10.1038/s41467-022-34823-3, 2022.

Wu, X., Wu, C., Lin, Z., and Yang, M.: Intra-seasonal variations of dust activity over East Asia in spring 2023 and their mechanisms, Global and Planetary Change, 244, 104638, https://doi.org/10.1016/j.gloplacha.2024.104638, 2025.

Xie, Q., Jia, X., Chen, X., and Qian, Q.: Combined effects of ocean-land processes on spring precipitation variability in Mongolian Plateau, Atmospheric Research, 313, 107765, https://doi.org/10.1016/j.atmosres.2024.107765, 2025.

Xing, Y., Liu, B., Wagner, L. E., and Qu, J.: Source shifting and contributions to Central East Asia dust events during 2000–2023, Sci. China Earth Sci., 68, 3804–3816, https://doi.org/10.1007/s11430-024-1706-5, 2025.

Xu, Y., Xu, X., and Tang, Q.: Human activity intensity of land surface: Concept, methods and application in China, J. Geogr. Sci., 26, 1349–1361, https://doi.org/10.1007/s11442-016-1331-y, 2016.

Yang, X., Yang, F., Zhou, C., Mamtimin, A., Huo, W., and He, Q.: Improved parameterization for effect of soil moisture on threshold friction velocity for saltation activity based on observations in the Taklimakan Desert, Geoderma, 369, 114322, https://doi.org/10.1016/j.geoderma.2020.114322, 2020.

https://doi.org/10.5194/egusphere-2026-3940
Preprint. Discussion started: 28 July 2026

Yang, Y., Qu, Z., Shi, P., Liu, L., Zhang, G., Tang, Y., Hu, X., Lv, Y., Xiong, Y., Wang, J., Shen, L., Lv, L., and Sun, S.: Wind regime and sand transport in the corridor between the Badain Jaran and Tengger deserts, central Alxa Plateau, China, Aeolian Research, 12, 143–156, https://doi.org/10.1016/j.aeolia.2013.12.006, 2014.

Yin, Z., Wan, Y., Zhang, Y., and Wang, H.: Why super sandstorm 2021 in North China?, National Science Review, 9, nwab165, https://doi.org/10.1093/nsr/nwab165, 2022.

Yu, T., Xiaole, P., Yujie, J., Yuting, Z., Weijie, Y., Hang, L., Shandong, L., and Zifa, W.: East Asia dust storms in spring 2021: Transport mechanisms and impacts on China, Atmospheric Research, 290, 106773, https://doi.org/10.1016/j.atmosres.2023.106773, 2023.

Zan, J., Maher, B. A., Fang, X., Stevens, T., Ning, W., Wu, F., Yang, Y., Kang, J., and Hu, Z.: Global dust impacts on biogeochemical cycles and climate, Nat Rev Earth Environ, 6, 789–807, https://doi.org/10.1038/s43017-025-00734-2, 2025.

Zhang, G., Wang, Y., Liu, L., Ma, Y., Lin, Z., Li, W., Zhang, T., Liu, S., Zhang, X., Wang, S., Liu, Z., Hu, J., and Shi, P.: Process, Causes, and Loss Assessment of the Extreme Wind-Dust Compound Disaster in China in April 2025, Int J Disaster Risk Sci, 16, 781–800, https://doi.org/10.1007/s13753-025-00668-9, 2025.

Zhang, Z. and Dong, Z.: Field observations of dust transport rates in Gobi deserts, Nat Hazards, 116, 1689–1709, https://doi.org/10.1007/s11069-022-05735-8, 2023.

Zhang, Z., Bird, A., Zhang, C., and Dong, Z.: Not all gravel deserts in northern China are sources of regionally deposited dust, Atmospheric Environment, 273, 118984, https://doi.org/10.1016/j.atmosenv.2022.118984, 2022.

Zhang, Z. C., Dong, Z. B., Pan, K. J., Zhang, Y., and Han, L. Y.: Characteristics of the Aeolian Sediments Transported Above a Gobi Surface, JGR Earth Surface, 129, e2024JF007736, https://doi.org/10.1029/2024JF007736, 2024.

Zhao, Y., Yue, X., Cao, Y., Zhu, J., Tian, C., Zhou, H., Chen, Y., Hu, Y., Fu, W., and Zhao, X.: Multi-model ensemble projection of the global dust cycle by the end of 21st century using the Coupled Model Intercomparison Project version 6 data, Atmos. Chem. Phys., 23, 7823–7838, https://doi.org/10.5194/acp-23-7823-2023, 2023.

Zhou, A., Zhao, W., Han, Y., Zhang, S., and Pereira, P.: Effects and benefits of wind erosion prevention in China's dryland and surrounding countries, CATENA, 251, 108812, https://doi.org/10.1016/j.catena.2025.108812, 2025a.

Zhou, W., Wang, H., and Ge, Q.: Contributions of climatic factors and vegetation cover to the temporal shift in Asian dust events, npj Clim Atmos Sci, 7, 328, https://doi.org/10.1038/s41612-024-00887-9, 2024.

Zhou, Y., Zhao, Y., Gao, X., Lei, J., and Dong, D.: Dust weather in Tarim Basin derived from a dust event on April 18–21, 2023, Atmospheric Pollution Research, 16, 102605, https://doi.org/10.1016/j.apr.2025.102605, 2025b.

Zhu, C., Wang, M., Meng, L., Mamtimin, A., Yang, F., Zhou, C., Pan, H., and Zhang, J.: Correlation between atmospheric boundary layer height and Concentration of dust aerosols in Taklimakan desert, Journal of Atmospheric and Solar-Terrestrial Physics, 277, 106677, https://doi.org/10.1016/j.jastp.2025.106677, 2025.